Journal of Materials Chemistry A

ROYAL SOCIETY OF CHEMISTRY

PAPER

View Article Online
View Journal | View Issue

Check for updates

Cite this: J. Mater. Chem. A, 2023, 11, 16846

Underlying potential evaluation of the real-process applications of magnetic porous liquids†

Hamidreza Mahdavi, [a] Muhammad M. Sadiq, [a] Stefan J. D. Smith,*[ab] Xavier Mulet*[ab] and Matthew R. Hill *[ab]

It is possible to engineer permanent pores into a liquid instead of transient intermolecular pores found in all liquids, and thereby design and form porous liquids (PLs). A combination of porosity and fluidity has garnered attention in recent years due to its exceptional physicochemical properties. In the years since the concept was introduced in 2007 and the first examples demonstrated in 2015, significant advances have been made in all three types of PLs. As a result of these advances, researchers now understand their structure and properties better, and interesting improvements in gas uptake and molecular separation have been made. Recently, Type III PLs have attracted attention as low-loss materials for continuous CO_2 capture that can be adapted to industrial applications and are easy to synthesise and create from a wide variety of MOFs and solvents, with possibilities of creating stable PLs through different MOF modification methods. In spite of these advances, the regeneration and reusability of PLs have not been thoroughly investigated. This work aims to systematically explore the possibilities of implementing PLs in real-process applications using magnetic framework composites (MFCs) as porogens with the aid of a compatible non-penetrating solvent. This provided insights into the static and dynamic sorption and desorption breakthrough isotherms and cyclic sorption and desorption properties. The MFCs ($MgFe_2O_4$@ZIF-62) with different concentrations of magnetic nanoparticles (1–6 wt% of magnetic nanoparticles to ZIF-62 mass) were combined with a compatible non-penetrating solvent to create magnetic porous liquids (MPLs). By using MFC triggering in PLs, it has been demonstrated using 3 cycles that gases can be reversibly captured and released. In this way, these nanoheaters overcome the thermal insulation property of porogens in Type III PLs. Therefore, the amount of CO_2 released during three sorption–desorption cycles remained relatively constant. MPL's regeneration energies for 3 cycles were among the lowest observed for any adsorbent. The MPL's low energy consumption and high productivity across 3 cycles exceed those of any previously reported adsorbent. These findings demonstrate the amazing cyclic sorption and desorption properties of the MPL's triggering release of the captured CO_2, which have numerous potential applications in gas separation.

Received 2nd May 2023
Accepted 11th July 2023

DOI: 10.1039/d3ta02602g

rsc.li/materials-a

Introduction

The last decade has seen a growing interest in low-cost carbon capture to tackle greenhouse gas emissions.[1] Carbon dioxide (CO_2) can be captured using various methods, such as membrane processes,[2] physical absorption,[3] porous material adsorption,[4] chemical absorption,[5] and hydrate carbon capture processes.[6] However, these processes have limitations, such as corrosion of equipment, high regeneration energy costs, low capacity, and requirements for high temperatures and pressures during operation.[7] In recent years, porous liquids (PLs) that combine both porosity and fluidity have gained attention for continuous carbon dioxide capture due to their exceptional physicochemical properties.[8] Based on the structure and composition of the porogen, PLs fall into three categories: Type I PLs consist of a single molecule with permanent pores; PLs of Type II contain a dissolved porogen in excluded solvents; and Type III PLs are porogens dispersed in a solvent that prevents the solvent from occupying the pores.[9–12] However, Type III PLs have recently attracted attention as a low-loss approach for continuous CO_2 capture that might be most applicable to industrial applications.[13]

Type III PLs can be made from a variety of porogen materials, such as metal–organic frameworks (MOFs), zeolites, porous carbon, silica nanoparticles, metal–organic polyhedra (MOPs), and covalent organic frameworks (COFs).[14–20] Porogens are primarily selected because their cavity windows are large enough to allow guest species to enter but too small for solvent

[a]Department of Chemical and Biological Engineering, Monash University, Clayton, VIC 3800, Australia. E-mail: matthew.hill@monash.edu

[b]CSIRO Manufacturing, Private Bag 10, Clayton South, VIC 3169, Australia

† Electronic supplementary information (ESI) available. See DOI: https://doi.org/10.1039/d3ta02602g

molecules to reach.[21,22] MOF structures have become the most widely used porogens in the formation of PLs because of their molecular-sized pores and a high degree of tunability.[23] As a subset of MOFs, Zeolitic Imidazolium Frameworks (ZIFs) are suitable potential candidates for use in PLs due to their small pore window, allowing the use of a broader range of solvents.[24] Solvents are also primarily selected for their non-penetrative properties with large molecular dimensions, incompatible shapes, suitable physical properties, and high scalability.[25,26] Solvents with large molecular dimensions are thus used to reduce the chances of the solvent penetrating through porous hosts, such as hydrocarbons, ionic liquid, liquid polymers, *etc.*[21,27–30] Hydrocarbon solvents with specific physical properties, like low volatility and viscosity, can be used in PLs.[22,31,32]

Although PLs are promising materials for CO_2 capture, the amount of energy required to regenerate the adsorbent/absorbent is one of the biggest obstacles to widespread use in industrial settings.[33–35] This issue may be addressed by a penetrating method that triggers the release of captured CO_2 from large quantities of PLs. As a result, it is imperative to engineer a PL to release the captured CO_2 after it absorbs the energy.[36] Some methods promote gas release from PLs such as chemical methods by inserting antagonistic guests such as chloroform or applying external stimuli methods such as ultrasonication. The chemical method is deemed unappealing for practical applications, primarily due to its irreversibility, unless the antagonistic guest is subsequently removed. On the other hand, the ultrasonication method is not as efficient as the addition of antagonistic guests. Moreover, they are not yet scalable or cost-effective.[37,38] Besides, pressure-swing or temperature-swing methods are also highly energy intensive.[36,39] Of course, it is possible to reduce the utilised energy by new approaches such as solar-radiation-induced adsorption/desorption systems which prove to be useful in MOF regeneration. However, the system's efficacy can be limited by the availability of sunlight and practicality in the liquid phase.[40] Furthermore, the latest advancements in PL regeneration provide evidence supporting the possibility of employing other external stimuli, such as light responsiveness. This method can be subject to light absorption by the liquid, limited passage of light within the liquid, and the possibility of photodegradation of the liquid and/or the MOFs.[41,42] Other external stimuli that have been recently applied to promote PL regeneration include shearing and heating. The efficacy of this method can be constrained by its sensitivity to fluctuations under environmental conditions, as well as concerns regarding its resilience over time.[43] Moreover, it was also discovered that more penetrating forms of radiation are preferred, as the light cannot be easily scaled.[44] Therefore, using different extrinsic species to prepare composites can be an effective way to give MOFs additional functionalities.[45,46] As one of the composites prepared with nanoparticles, magnetic framework composites (MFCs) respond efficiently to external stimuli due to their interaction with an external magnetic field.[47,48] Therefore, it is important to investigate the possibilities of creating PLs with MFCs.

This work focuses on creating magnetic porous liquids (MPLs) using MFCs and a non-penetrating solvent for the first time. MFCs with different concentrations of magnetic nanoparticles (1 wt%, 3 wt% and 6 wt% of magnetic nanoparticles to ZIF-62 mass) and 1,3,5-triisopropylbenzene (TPB) have been used to study the possibility of MPL formation and then the impact of magnetic nanoparticle concentration on sorption and desorption characteristics. ZIF-62 not only forms a stable PL with TPB, but its synthesis procedure also makes it easily adjustable to incorporate magnetic nanoparticles. ZIF-62 is also a stable and long-lasting choice throughout the magnetic induction swing adsorption process due to its strong thermal and chemical stability. After exposure to extended solvents, the tested MFCs were recovered to confirm that they were not affected. Furthermore, high-pressure (10 bar) gas sorption measurements of solvent were taken and compared to corresponding MFC–solvent combinations (10 wt% of MFC to solvent) to measure porosity. The findings indicated that MPLs could be used in CO_2 gas scrubbing applications due to their amazing cyclic sorption and desorption properties.

Experimental

The nano-sized MFCs ($MgFe_2O_4$@ZIF-62) containing different amounts of magnetic nanoparticles (1 wt%, 3 wt% and 6 wt% of magnetic nanoparticles to ZIF-62 mass) were synthesised as porogens (Fig. 1, see ESI Section S2† for details). The synthesis was confirmed to have succeeded by using Fourier-transform infrared spectroscopy (FTIR), powder X-ray diffraction (PXRD), thermogravimetric analysis (TGA), low-pressure gas sorption, scanning electron microscopy (SEM), vibrating sample magnetometer (VSM), inductively coupled plasma (ICP), X-ray photoelectron spectroscopy (XPS), and solid-state nuclear magnetic resonance (13C NMR). Besides, TPB (Bp: 232–236 °C) was also selected as a solvent because of its physicochemical properties (Table S1†). The porogens were added to the solvent at a concentration of 1 wt%, 2.5 wt%, 5 wt%, and 10 wt% and sonicated to form an initial dispersion. Fig. S3 and S4† provide more details regarding the solvents used and the preparation of the MFC-solvent combinations, respectively. The MFC–solvent combinations were evaluated as liquid adsorbents and compared based on viscosity, density, high-pressure gas sorption, and static and dynamic gas sorption and desorption. MFCs from the 10 wt% MFC–solvent combination were recovered *via* solvent exchange with methanol, centrifugation, washing in triplicate, and overnight vacuum drying at 100 °C. Following the recovery of the MFCs, they were characterised and compared to as-synthesised MFCs based on their chemical bonding, crystal structure, thermal stability, magnetic properties, magnetic

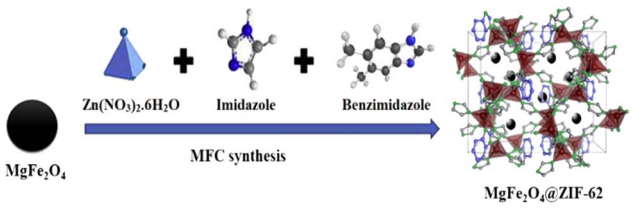

Fig. 1 Images of nano-sized ZIF-62, and MFC derivative.

nanoparticle content, binding energy and elemental composition, chemical structure, surface area, pore size, and morphology. For clarity, this manuscript follows the naming convention of 'magnetic nanoparticle concentration in MFC% $MgFe_2O_4$@ZIF-$62_{MFC\ concentration\ in\ solvent\%}$-solvent', (*e.g.*: 1% $MgFe_2O_4$@ZIF-$62_{10\%}$-TPB) for the prepared liquids, while ZIFs recovered from combinations are denoted as 'magnetic nanoparticle concentration in MFC% $MgFe_2O_4$@ZIF-$62_{EX\text{-}Solvent}$' (*e.g.*: 1% $MgFe_2O_4$@ZIF-$62_{EX\text{-}TPB}$).

Results and discussion

MFC and recovered MFC characterisation

The MFCs were recovered from the solvent to study the effects of solvent exposure using the same techniques (detailed information is provided in ESI Fig. S5–S13†). Based on FTIR spectra, it can be concluded that the structural group was retained in the MFCs, and recovered MFCs. It has also been confirmed through XRD patterns and TGA results, respectively, that MFCs and recovered MFCs retained their crystal structures and thermal stabilities. The combination of magnetic nanoparticles in ZIF-62 led to a decrease in surface area, maximum N_2 adsorption capacity and a slight increase in pore sizes in the MFCs. The recovered MFCs showed a small reduction in surface area, maximum N_2 adsorption capacity, and the number of pores. According to the SEM images, the morphology of MFCs and recovered MFCs mostly remained unchanged. However, it was observed that the magnetic nanoparticles surrounding MFCs were lost. This phenomenon may be explained by the fact that to recover the MFCs from TPB, the intermolecular bonds between them need to be broken, which results in the pores collapsing. Furthermore, MFC pores may not respond well to solvent removal and may collapse due to the drying conditions used to recover the MFCs. The VSM and ICP analysis results confirm the magnetic properties of MFCs and recovered MFCs and remaining magnetic nanoparticles incorporated into the structure. A slight reduction in the magnetic properties has been observed due to the loss of magnetic nanoparticles surrounding MFCs, agreeing with what was observed in SEM images. XPS and ^{13}C NMR results indicate that the binding energies and chemical structure in the MFCs and recovered MFCs were almost unchanged. However, since XPS is a surface analysis technique, the elemental composition significantly reduces. This is due to the loss of magnetic nanoparticles surrounding MFCs.

Mechanistic insights to design

The wide range of MOFs and solvents, combined with various modification methods, has led to a large number of well-defined MOF-based PL formulations. However, a significant concern for their widespread use in industrial settings is the high energy required to regenerate the adsorbent and absorbent components of PLs. The challenge of high regeneration energy demands must be overcome for processable PLs with acceptable viscosity, open porosity with good capacities, and guest solubility kinetics. Magnetic framework composites were investigated to establish whether or not MFC-based PL formation was possible and then to determine the parametric space where functional PLs can be utilised in real-world applications. Future research on PLs could benefit significantly from this study's findings.

Viscosity

The viscosity measures friction within the liquid, which presents resistance to its flow. Thus, PL's viscosity is an essential factor in liquid handling settings. MFCs act as obstacles that cause higher friction in the solvent, making the MFC–solvent combinations less likely to flow freely and increasing their resistance. As a result, liquid dispersions have higher viscosities than pure solvents as shown in Fig. 2 (Fig. S9, and Table S6†). However, even with the increased viscosity of the MFC–solvent combinations, their viscosities are still low enough (less than 0.2797 cP) to allow them to be utilised in typical pumps for industry. A high degree of compatibility between MFCs and solvent can explain this result.

Density

The density is the mass ratio to volume or mass per unit volume. A PL's density is essentially a measure of how much mass exists in a volume, decreasing when more space is introduced. The lower measured density than predicted implies that the MFC–solvent combinations have a greater porosity level than the associated solvent. A comparison of the measured and predicted densities can be seen in Fig. 2 (more information is in Fig. S10, and Table S7†). Although the measured and predicted values seem similar, measurements are below the confidence interval for the predictions, indicating permanent porosity and preventing solvent penetration into the pores of the MFCs. A

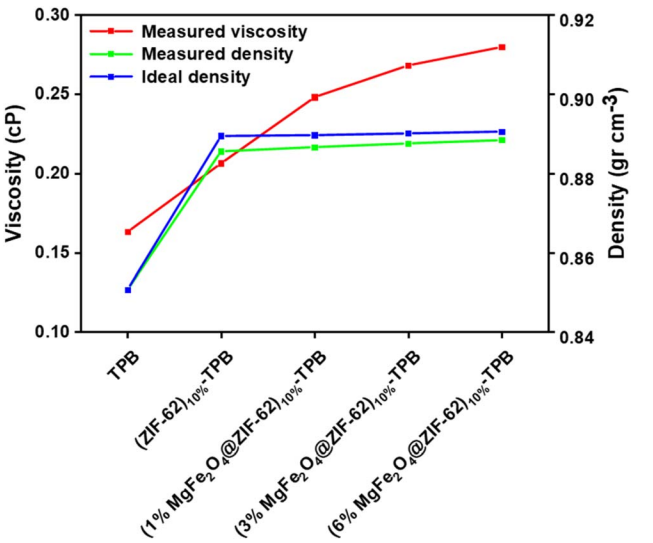

Fig. 2 Measured viscosity, ideal and measured densities of ZIF-$62_{10\%}$-TPB as control, and MPLs with 10% MFCs containing different magnetic nanoparticle concentrations (1 wt%, 3 wt% and 6 wt% of magnetic nanoparticles to ZIF-62 mass) compared to the solvent (the order of standard deviation values is <5%).

significant difference in behaviour was not found between the MFC–solvent combinations.

High-pressure gas sorption

High-pressure gas sorption can be a useful tool for determining the properties of microporous materials used for gas separation. PLs' permanent porosity can improve their sorption capabilities by providing additional free volume. As presented in Fig. 3 (more information is in Fig. S11†), the CO_2 adsorption of TPB and ZIF-$62_{10\%}$-TPB at 2 bar was 0.58 mmol g^{-1} and 0.85 mmol g^{-1}, respectively. These observations agree well with the presence of additional free volume. Furthermore, (1%, 3% and 6% $MgFe_2O_4$@ZIF-62)$_{10\%}$-TPB MPLs have also demonstrated high adsorption capacities compared to the solvent (0.62 mmol g^{-1}, 0.74 mmol g^{-1}, and 0.81 mmol g^{-1}, respectively). Although MFCs with increasing concentrations of magnetic nanoparticles will have lower adsorption capacities, they still outperform pure solvents in their uptake capacity. It is evident from all investigated samples that MPLs have guest-accessible porosity, as determined by their improved gas adsorption capacities.

Static and dynamic gas sorption and desorption breakthrough isotherms

The static and dynamic triggered release of captured CO_2 from the MPLs was investigated through a combination of an induction heating machine and adsorption equipment (Fig. S12†). The CO_2 sensor box was initially filled with a mixed gas containing CO_2 : N_2 by the composition of 15 : 85 v/v%. The mixed gas was then continuously introduced to the PMLs. As a result, sorption breakthrough isotherms were obtained. The CO_2 sensor box was purged of CO_2 with a flow of He gas before the breakthrough isotherms were collected. Then, the coils of the induction heating machine were subjected to a high voltage to create a large magnetic field, which caused the MFCs to be heated to the maximum temperature. Additionally, He gas has been used to sweep away the released CO_2. The desorption breakthrough isotherms were thus obtained. This method allowed us to investigate gas sorption/desorption cycles for the MPLs without the obvious disadvantages of low performance, not being scalable, not being cost-effective, having to add and then remove an antagonistic guest, and using an extensive amount of energy.[37,38]

Static gas sorption and desorption CO_2 isotherms of the MPLs are presented in Fig. 4 (Table S8†). It can be observed in Fig. 4a that the sorption capacity of (ZIF-62)$_{10\%}$-TPB was greater than that of TPB which provides evidence for the formation of the PL. On the other hand, the sorption capacity of MPLs was found to be greater than that of TPB which supports the presence of permanent porosity, but lower than that of (ZIF-62)$_{10\%}$-TPB. This is because the increase in magnetic nanoparticle concentration leads to a decrease in porosity and active surface area for sorption.[36,49,50] Moreover, with the increasing concentration of magnetic nanoparticles in the MPLs, an increase in the variance of sorption capacity between (ZIF-62)$_{10\%}$-TPB and MPLs was observed. This observation is consistent with the high-pressure gas sorption results. Moreover, as shown in

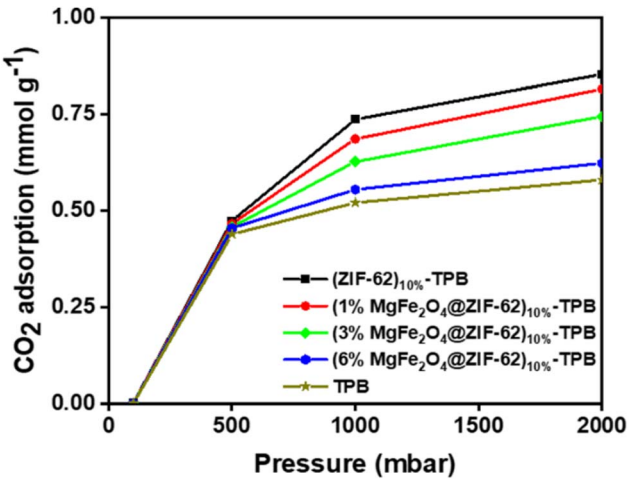

Fig. 3 The CO_2 sorption capacity of TPB, and (ZIF-62)$_{10\%}$-TPB as controls, and MPLs with 10% MFCs containing different magnetic nanoparticle concentration (1 wt%, 3 wt% and 6 wt% of magnetic nanoparticles to ZIF-62 mass) using pure CO_2 at 298 K.

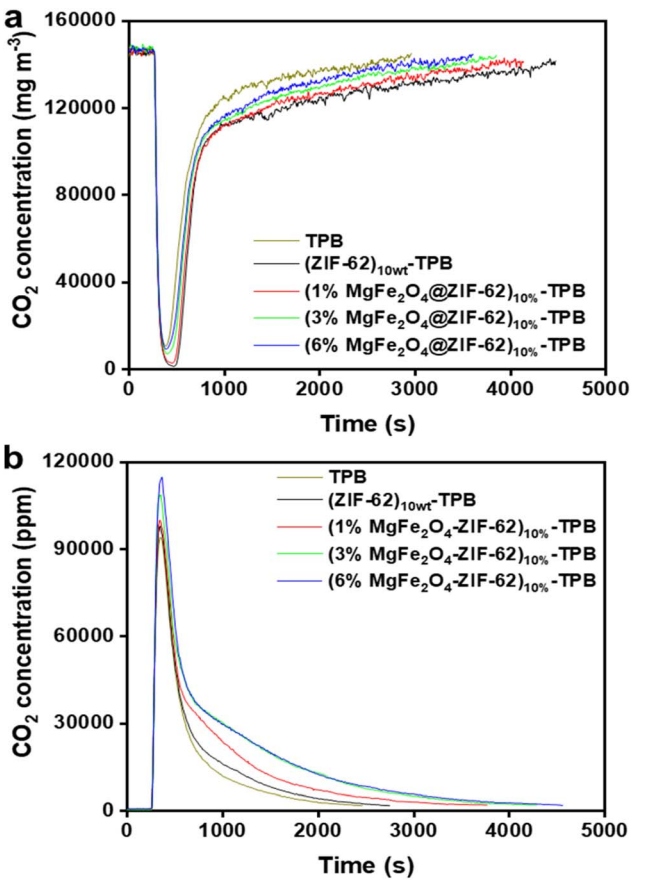

Fig. 4 The static gas sorption (magnetic field off) and desorption (magnetic field on) breakthrough of TPB, and (ZIF-62)$_{10\%}$-TPB as controls, and MPLs with 10% MFCs containing different magnetic nanoparticle concentration (1 wt%, 3 wt% and 6 wt% of magnetic nanoparticles to ZIF-62 mass) using the mixed gas CO_2 : N_2 (15 : 85, v/v%) at 298 K.

Fig. 4b, using He as a sweeping gas and applying an induction process, which caused the temperature of TPB to rise, both result in the partial releasing of the adsorbate CO_2 from the TPB and liquid phase of the other combinations. However, the CO_2 desorption of $(ZIF\text{-}62)_{10\%}$-TPB was lower than that of TPB due to the inability of the sweeping gas and applying the induction process to release the adsorbate CO_2 from ZIF-62 pores, whereas the CO_2 removal increased with increasing concentration of magnetic nanoparticles. Thus, the triggered release of captured CO_2 from MFCs can be attributed to the MFCs being irradiated with a magnetic field which increases the surface energy of the composite. Ergo, the intermolecular interactions between CO_2 molecules and MFC surfaces are weakened, triggering the immediate release of captured CO_2. As magnetic nanoparticle concentration increases, more and stronger irradiation of MFCs in the magnetic field occurs, which will result in more CO_2 being released (Fig. 4b and Table S8†).[39,44,51] Consequently, there is a trade-off between MPLs' sorption and desorption capabilities depending on the concentration of magnetic nanoparticles present in the MFCs.[38] Therefore, for the purpose of cycling gas sorption and desorption experiments, and energy-efficient MPL regeneration comparisons, the $(3\%\ MgFe_2O_4@ZIF\text{-}62)_{10\%}$-TPB was selected.

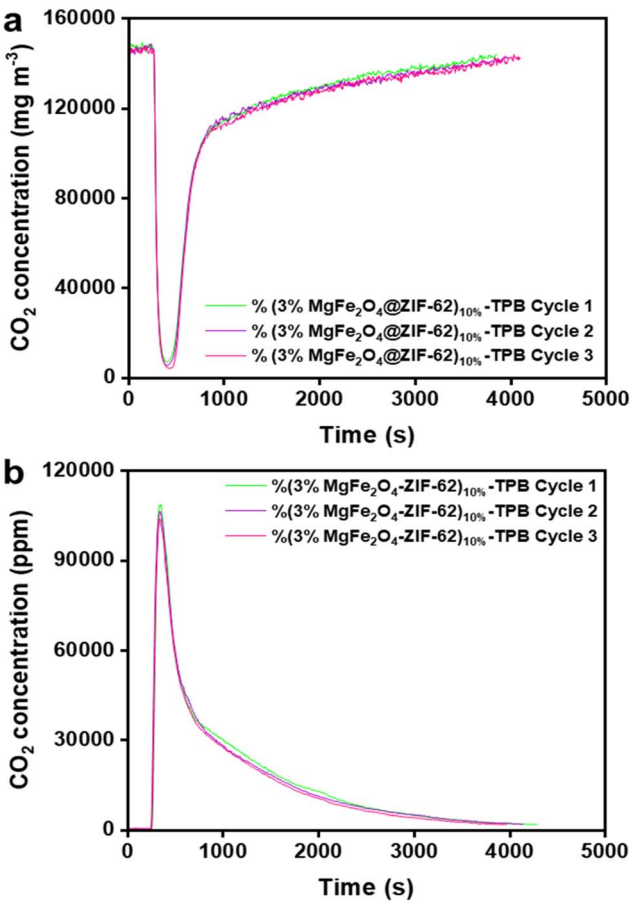

Fig. 5 The dynamic gas sorption (magnetic field off) and desorption (magnetic field on) breakthrough of $(3\%\ MgFe_2O_4@ZIF\text{-}62)_{10\%}$-TPB using the mixed gas CO_2 : N_2 (15 : 85, v/v%) at 298 K.

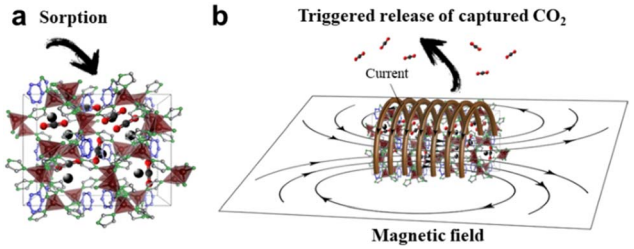

Fig. 6 The schematic of CO_2 gas (a) sorption into, and (b) the proposed concept for CO_2 sorption and release from MPLs.

Fig. 5 (Table S9†) presents the dynamic gas sorption and desorption breakthrough isotherms of CO_2 from MPLs. To examine the effectiveness of the MPLs in the magnetic induction swing adsorption process, the MPLs were irradiated with an AC magnetic field periodically during the sorption phase. As shown in Fig. 5a and 6a, sorption began when the magnetic field was off. However, Fig. 5b and 6b illustrate that when the magnetic field was on, the periodic irradiation of MPLs induced localised heating in MFCs through the incorporated magnetic nanoparticle. This leads to an increase in temperature, which impairs intermolecular interactions between CO_2 molecules and the adsorbent surface, resulting in rapid CO_2 release.[36,39,51,52] The CO_2 released remained relatively constant during three gas sorption–desorption cycles. Therefore, the 3 cycles demonstrate the feasibility of the reversible capture and release of gases using MFC triggers in PLs. Consequently, these local nano heaters can be used to overcome the thermal insulation property of porogens in Type III PLs, which has the potential for widespread application in gas separation applications.

Energy-efficient MPL regeneration

The effectiveness of the triggered release of captured CO_2 from MPL using the induction process over 3 consecutive cycles was assessed through a comparison of the MPL regeneration energy against other porous adsorbent materials. Fig. 7a shows the results of the analysis of the regeneration energy. At the magnetic fields, the regeneration energies calculated for MPL for 3 consecutive cycles were 0.2771, 0.2834, and 0.3032 MJ kg $CO_2{}^{-1}$, respectively. As shown, the MPL system's regeneration energy is much lower than that required by TPB, $(ZIF\text{-}62)_{10\%}$-TPB, and other adsorbent materials. Moreover, the productivity and energy consumption also demonstrate the potential of MPL when used to trigger the release of captured CO_2. Fig. 7b depicts the productivity and energy consumption throughout the 3 cycles. At the magnetic fields, the productivities calculated for MPL for the 3 consecutive cycles were 0.2800, 0.2786, and 0.2779 kg CO_2 h^{-1} kg MPL^{-1}, respectively, whereas the energy consumption values were 0.0770, 0.0787, and 0.0842 kW h kg $CO_2{}^{-1}$. As shown in Fig. 7, compared to TPB, $(ZIF\text{-}62)_{10\%}$-TPB, and other adsorbent materials, the MPL system's productivity is high while the energy consumption is low. As far as can be determined, the regeneration energies calculated of MPL for 3 consecutive cycles were some of the lowest reported for any

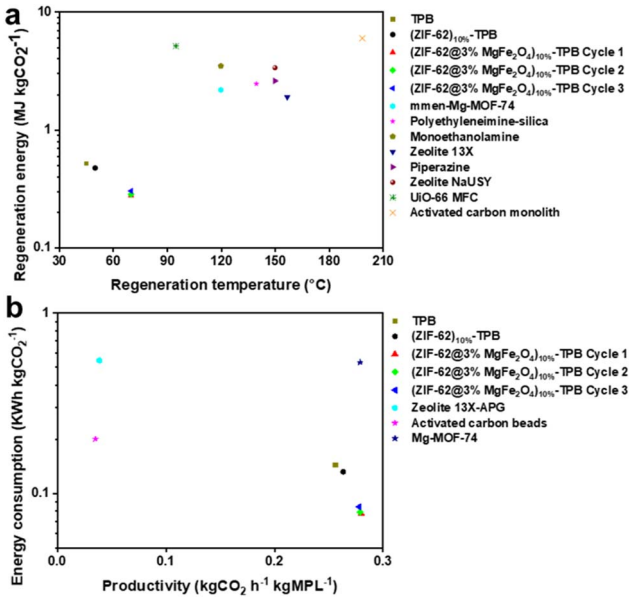

Fig. 7 (a) Regeneration energy (MJ kg CO_2^{-1}) as a function of regeneration temperature (°C) for MPL *vs.* stated literature values including zeolite NaUSY,[53] zeolite 13X,[54] activated carbon monolith,[55] polyethyleneimine-silica,[56] piperazine,[57] monoethanolamine,[58,59] mmen-Mg-MOF-74,[60] and UiO-66 MFC.[39] (b) Energy consumption (kJ kg CO_2^{-1}) as a function of productivity (kg CO_2 h^{-1} kg Ads^{-1}) for MPL *vs.* stated literature values including zeolite 13X-APG,[61] activated carbon beads,[62] and Mg-MOF-74.[63]

adsorbent. Furthermore, MPL has a low energy consumption and great productivity across 3 consecutive cycles, surpassing any adsorbent with previously reported values. These results confirm the effectiveness of the triggered release of captured CO_2 from MPL using the induction process.

Conclusions

Regeneration and reusability of PL remain nearly unexplored despite these advances. In this study, MFCs were used as a porogen with a non-penetrating solvent to assess the feasibility of implementing PLs in real-world applications. These experiments provided insights into static and dynamic sorption and desorption isotherms and cyclic sorption and desorption properties. It was confirmed that the MPLs are formed in the presence of MFCs due to the higher sorption than the solvent when using the induction heating machine and the adsorption equipment. This was also consistent with the results of the high-pressure gas sorption and density measurements. Although advances have been made in the development of PLs, the comprehensive exploration of their regeneration and reusability remains an area that requires further examination. By increasing the concentration of magnetic nanoparticles, the CO_2 sorption capacity was reduced. Since there are more magnetic nanoparticles, there is less porosity and surface area available for sorption. Furthermore, pure solvent CO_2 desorption was lower than that of MPLs, which increased with increasing concentration of magnetic nanoparticles. The triggered release of captured CO_2 can be explained by MFCs being exposed to the magnetic field, which increases the surface energy of the composite. As a result, intermolecular interactions between CO_2 molecules and MFC surfaces weakened, triggering an immediate release of captured CO_2. When the concentration of magnetic nanoparticles in the magnetic field increases, more and stronger irradiation of MFCs occurs, resulting in higher CO_2 desorption. The MPLs were periodically exposed to AC magnetic fields during the sorption to examine their efficiency in the magnetic induction swing adsorption process. Gas capture and release can be reversible with MFC triggering in PLs. The porogens in Type III PLs have thermal insulation, but these nano heaters overcome it. Therefore, the CO_2 released over three sorption–desorption cycles remained relatively constant. To the best of our knowledge, the regeneration energies computed for MPL for 3 cycles in a sequence were among the lowest of any adsorbent that was reported. In addition, MPL has a low energy consumption and remarkable productivity during three consecutive cycles, which surpasses any other adsorbent that has previously reported values. These findings provide further evidence that the MPL's induction process is an efficient means of triggering the release of the captured CO_2. As a result of their extraordinary cyclic sorption and desorption properties, MPLs have an incredible range of potential applications in gas separation especially post-combustion capture of CO_2.

Author contributions

H. M. led the project administration, conceptual and experimental design, analysis, interpretation of results, and writing of the draft. M. M. S., S. J. D. S., X. M., and M. R. H. contributed to the project administration, conceptual and experimental design, analysis, and interpretation of results.

Conflicts of interest

There are no conflicts to declare.

Acknowledgements

The authors acknowledge the use of facilities within the Monash X-ray Platform and Monash Centre for Electron Microscopy.

References

1 E. Martin-Roberts, V. Scott, S. Flude, G. Johnson, R. S. Haszeldine and S. Gilfillan, *One Earth*, 2021, **4**, 1569–1584.
2 J. Xu, Z. Wang, Z. Qiao, H. Wu, S. Dong, S. Zhao and J. Wang, *J. Membr. Sci.*, 2019, **581**, 195–213.
3 H. Zhai and E. S. Rubin, *Environ. Sci. Technol.*, 2018, **52**, 4996–5004.
4 X.-q. Zhang, W.-c. Li and A.-h. Lu, *New Carbon Mater.*, 2015, **30**, 481–501.
5 J. Oexmann, A. Kather, S. Linnenberg and U. Liebenthal, *Greenhouse Gases: Sci. Technol.*, 2012, **2**, 80–98.

6 K. M. Sabil and B. Partoon, *Curr. Opin. Green Sustainable Chem.*, 2018, **11**, 22–26.
7 H. Li, B. Liu, M. Yang, D. Zhu, Z. Huang, W. Chen, L. Yang and G. Chen, *Ind. Eng. Chem. Res.*, 2020, **59**, 6154–6163.
8 H. R. Mahdavi, S. J. D. Smith, X. Mulet and M. R. Hill, *Mater. Horiz.*, 2022, **9**, 1577–1601.
9 W. Shan, P. F. Fulvio, L. Kong, J. A. Schott, C.-L. Do-Thanh, T. Tian, X. Hu, S. M. Mahurin, H. Xing and S. Dai, *ACS Appl. Mater. Interfaces*, 2018, **10**, 32–36.
10 J. Zhang, S.-H. Chai, Z.-A. Qiao, S. M. Mahurin, J. Chen, Y. Fang, S. Wan, K. Nelson, P. Zhang and S. Dai, *Angew. Chem., Int. Ed.*, 2015, **54**, 932–936.
11 N. O'Reilly, N. Giri and S. L. James, *Chem. – Eur. J.*, 2007, **13**, 3020–3025.
12 S. J. D. Smith, C. D. Wood, P. H. M. Feron, H. Mahdavi, R. J. Mulder, C. M. Doherty, M. R. Hill and X. Mulet, *Sci. China Mater.*, 2022, **65**, 1937–1942.
13 T. Nakanishi, *Functional Organic Liquids*, Wiley, 2019.
14 P. A. Wright and R. S. o. Chemistry, *Microporous Framework Solids*, RSC Publishing, 2008.
15 A. K. Cheetham, G. Férey and T. Loiseau, *Angew. Chem., Int. Ed.*, 1999, **38**, 3268–3292.
16 J.-R. Li, R. J. Kuppler and H.-C. Zhou, *Chem. Soc. Rev.*, 2009, **38**, 1477–1504.
17 A. G. Slater and A. I. Cooper, *Science*, 2015, **348**, aaa8075.
18 Z. Deng, W. Ying, K. Gong, Y.-J. Zeng, Y. Yan and X. Peng, *Small*, 2020, **16**, 1907016.
19 R. E. Mow, A. S. Lipton, S. Shulda, E. A. Gaulding, T. Gennett and W. A. Braunecker, *J. Mater. Chem. A*, 2020, **8**, 23455–23462.
20 J. Cahir, M. Y. Tsang, B. Lai, D. Hughes, M. A. Alam, J. Jacquemin, D. Rooney and S. L. James, *Chem. Sci.*, 2020, **11**, 2077–2084.
21 R. J. Kearsey, B. M. Alston, M. E. Briggs, R. L. Greenaway and A. I. Cooper, *Chem. Sci.*, 2019, **10**, 9454–9465.
22 H. Mahdavi, H. Zhang, L. K. Macreadie, C. M. Doherty, D. Acharya, S. J. D. Smith, X. Mulet and M. R. Hill, *Nano Res.*, 2022, **15**, 3533–3538.
23 H.-C. J. Zhou and S. Kitagawa, *Chem. Soc. Rev.*, 2014, **43**, 5415–5418.
24 K. S. Park, Z. Ni, A. P. Côté, J. Y. Choi, R. Huang, F. J. Uribe-Romo, H. K. Chae, M. O'Keeffe and O. M. Yaghi, *Proc. Natl. Acad. Sci. U. S. A.*, 2006, **103**, 10186.
25 U. Vagt and C. Emmanuel, *Chem. Process.*, 2006, **69**, 45–49.
26 A. B. Bourlinos, S. Ray Chowdhury, R. Herrera, D. D. Jiang, Q. Zhang, L. A. Archer and E. P. Giannelis, *Adv. Funct. Mater.*, 2005, **15**, 1285–1290.
27 N. Giri, C. E. Davidson, G. Melaugh, M. G. Del Pópolo, J. T. A. Jones, T. Hasell, A. I. Cooper, P. N. Horton, M. B. Hursthouse and S. L. James, *Chem. Sci.*, 2012, **3**, 2153–2157.
28 S. James, M. Y. Tsang, J. Cahir, D. Rooney, Porous liquids 2017, *US. Pat.*, No. 2020/0330919 A1, 2020.
29 H. Liu, B. Liu, L.-C. Lin, G. Chen, Y. Wu, J. Wang, X. Gao, Y. Lv, Y. Pan, X. Zhang, X. Zhang, L. Yang, C. Sun, B. Smit and W. Wang, *Nat. Commun.*, 2014, **5**, 5147.
30 B. Lai, J. Cahir, M. Y. Tsang, J. Jacquemin, D. Rooney, B. Murrer and S. L. James, *ACS Appl. Mater. Interfaces*, 2021, **13**, 932–936.
31 H. Mahdavi, N. T. Eden, C. M. Doherty, D. Acharya, S. J. D. Smith, X. Mulet and M. R. Hill, *ACS Appl. Mater. Interfaces*, 2022, **14**, 23392–23399.
32 H. Mahdavi, J. Burdloff, A. Robin, S. J. D. Smith, X. Mulet and M. R. Hill, *ACS Mater. Lett.*, 2023, **5**, 549–557.
33 K. Sumida, D. L. Rogow, J. A. Mason, T. M. McDonald, E. D. Bloch, Z. R. Herm, T.-H. Bae and J. R. Long, *Chem. Rev.*, 2012, **112**, 724–781.
34 D. M. D'Alessandro, B. Smit and J. R. Long, *Angew. Chem., Int. Ed.*, 2010, **49**, 6058–6082.
35 P. Falcaro, R. Ricco, A. Yazdi, I. Imaz, S. Furukawa, D. Maspoch, R. Ameloot, J. D. Evans and C. J. Doonan, *Coord. Chem. Rev.*, 2016, **307**, 237–254.
36 H. Li, M. M. Sadiq, K. Suzuki, R. Ricco, C. Doblin, A. J. Hill, S. Lim, P. Falcaro and M. R. Hill, *Adv. Mater.*, 2016, **28**, 1839–1844.
37 A. I. Cooper, *ACS Cent. Sci.*, 2017, **3**, 544–553.
38 R. L. Greenaway, D. Holden, E. G. B. Eden, A. Stephenson, C. W. Yong, M. J. Bennison, T. Hasell, M. E. Briggs, S. L. James and A. I. Cooper, *Chem. Sci.*, 2017, **8**, 2640–2651.
39 M. M. Sadiq, H. Li, A. J. Hill, P. Falcaro, M. R. Hill and K. Suzuki, *Chem. Mater.*, 2016, **28**, 6219–6226.
40 C. Gu, P. Tan, T.-Y. Jiang, X.-Q. Wang, B. Hu, X.-Q. Liu and L.-B. Sun, *Cell Rep. Phys. Sci.*, 2022, **3**, 101122.
41 M. K. Dinker, K. Zhao, Z. Dai, L. Ding, X.-Q. Liu and L.-B. Sun, *Angew. Chem., Int. Ed.*, 2022, **61**, e202212326.
42 M. C. Brand, N. Rankin, A. I. Cooper and R. L. Greenaway, *Chem. – Eur. J.*, 2023, **29**, e202202848.
43 X. Li, D. Wang, Z. He, F. Su, J. Zhang, Y. Wang, Y. Xin, H. Wang, D. Yao, M. Li and Y. Zheng, *J. Mater. Chem. A*, 2022, **10**, 13333–13344.
44 R. Lyndon, K. Konstas, B. P. Ladewig, P. D. Southon, P. C. J. Kepert and M. R. Hill, *Angew. Chem., Int. Ed.*, 2013, **52**, 3695–3698.
45 G. Lu, S. Li, Z. Guo, O. K. Farha, B. G. Hauser, X. Qi, Y. Wang, X. Wang, S. Han, X. Liu, J. S. DuChene, H. Zhang, Q. Zhang, X. Chen, J. Ma, S. C. J. Loo, W. D. Wei, Y. Yang, J. T. Hupp and F. Huo, *Nat. Chem.*, 2012, **4**, 310–316.
46 J. Tang, R. R. Salunkhe, J. Liu, N. L. Torad, M. Imura, S. Furukawa and Y. Yamauchi, *J. Am. Chem. Soc.*, 2015, **137**, 1572–1580.
47 R. Ricco, L. Malfatti, M. Takahashi, A. J. Hill and P. Falcaro, *J. Mater. Chem. A*, 2013, **1**, 13033–13045.
48 L. H. Reddy, J. L. Arias, J. Nicolas and P. Couvreur, *Chem. Rev.*, 2012, **112**, 5818–5878.
49 S.-S. Chen, S.-S. Han, C.-B. Ma, W.-D. Li and Y. Zhao, *Cryst. Growth Des.*, 2021, **21**, 869–885.
50 H. Li and M. R. Hill, *Acc. Chem. Res.*, 2017, **50**, 778–786.
51 H. Li, M. M. Sadiq, K. Suzuki, C. Doblin, S. Lim, P. Falcaro, A. J. Hill and M. R. Hill, *J. Mater. Chem. A*, 2016, **4**, 18757–18762.
52 Y. Tao, G. Huang, H. Li and M. R. Hill, *ACS Sustainable Chem. Eng.*, 2019, **7**, 13627–13632.

53 A. Ntiamoah, J. Ling, P. Xiao, P. A. Webley and Y. Zhai, *Ind. Eng. Chem. Res.*, 2016, **55**, 703–713.
54 C. A. Grande, R. P. Ribeiro, E. L. Oliveira and A. E. Rodrigues, *Energy Procedia*, 2009, **1**, 1219–1225.
55 C. A. Grande and A. E. Rodrigues, *Int. J. Greenhouse Gas Control*, 2008, **2**, 194–202.
56 W. Zhang, H. Liu, Y. Sun, J. Cakstins, C. Sun and C. E. Snape, *Appl. Energy*, 2016, **168**, 394–405.
57 G. Rochelle, E. Chen, S. Freeman, D. Van Wagener, Q. Xu and A. Voice, *Chem. Eng. J.*, 2011, **171**, 725–733.
58 M. R. M. Abu-Zahra, J. P. M. Niederer, P. H. M. Feron and G. F. Versteeg, *Int. J. Greenhouse Gas Control*, 2007, **1**, 135–142.
59 M. E. Boot-Handford, J. C. Abanades, E. J. Anthony, M. J. Blunt, S. Brandani, N. Mac Dowell, J. R. Fernández, M.-C. Ferrari, R. Gross and J. P. Hallett, *Energy Environ. Sci.*, 2014, **7**, 130–189.
60 T. M. McDonald, J. A. Mason, X. Kong, E. D. Bloch, D. Gygi, A. Dani, V. Crocella, F. Giordanino, S. O. Odoh and W. S. Drisdell, *Nature*, 2015, **519**, 303–308.
61 L. Wang, Y. Yang, W. Shen, X. Kong, P. Li, J. Yu and A. E. Rodrigues, *Chem. Eng. Sci.*, 2013, **101**, 615–619.
62 C. Shen, Z. Liu, P. Li and J. Yu, *Ind. Eng. Chem. Res.*, 2012, **51**, 5011–5021.
63 R. Ben-Mansour and N. A. A. Qasem, *Energy Convers. Manage.*, 2018, **156**, 10–24.